

## Supporting Information

### Regulating the Electronic States of NiSe<sub>2</sub> by Cr-doping to Promote Formation of Active Phase for High Catalytic Performance of Urea Oxidation Reaction

Shao-Lan Zheng<sup>†</sup>, Hui-Min Xu<sup>†</sup>, Chen-Jin Huang<sup>†</sup>, Hong-Rui Zhu, Chen-Yu Song, Ruo-Zhen Xiong, Gao-Ren Li\*

*College of Materials Science and Engineering, Sichuan University, Chengdu 610065, China*

<sup>†</sup>These authors contributed equally: Shao-Lan Zheng, Hui-Min Xu, Chen-Jin Huang

E-mail: [ligaoren@scu.edu.cn](mailto:ligaoren@scu.edu.cn)

#### Experimental section

##### Chemical reagents and materials

The chemical reagents and materials utilized in this work were all received from the manufacturer. Selenium (Se power, 99.99%, Macklin) was acquired from Shanghai Macklin Biochemical Technology Co., LTD. Chromium(III) nitrate nonahydrate (CrN<sub>3</sub>O<sub>9</sub>·9H<sub>2</sub>O, 99.0%, Aladdin) was sourced from Shanghai Aladdin Biochemical Technology Co Ltd. Urea (H<sub>2</sub>NCONH<sub>2</sub>, 99%, Aladdin) was sourced from Shanghai Aladdin Biochemical Technology Co Ltd. Nickel(II) nitrate hexahydrate (Ni(NO<sub>3</sub>)<sub>2</sub>·6H<sub>2</sub>O, AR, Keshi) was procured from Chengdu Chron Chemicals Co., LTD. Nickel foam (NF) was procured from Shenzhen Kejing Zhida Technology Co., LTD. The NF's thickness measured 1.6 mm, and its surface density was 350 g·m<sup>-2</sup>. Deionized (DI) and ultra-pure water were generated by an ultrapure water system. All reagents were employed without additional purification.

##### Methods

Firstly, NF (1 cm × 2 cm) was soaked in 3.0 M HCl solution for ultrasonic cleaning for 15 min, followed by ultrasonic cleaning in ethanol and UP water for 15 min to remove oxide impurities on NF. The specific

experimental steps were as follows: 1 mmol  $\text{Ni}(\text{NO}_3)_2 \cdot 6\text{H}_2\text{O}$ ,  $x$  mmol  $\text{Cr}(\text{NO}_3)_3 \cdot 9\text{H}_2\text{O}$  ( $x = 0.1, 0.25, 0.4$ ), and 0.2 g  $\text{CO}(\text{NH}_2)_2$  are dissolved in 30 mL of deionized water and stirred evenly for 30 min, and then transferred to a 50 mL stainless steel PTFE autoclave. Then place three pieces of the pretreated NF sheets in a reaction vessel and maintain at 150 °C for 12 h. After natural cooling, the samples were washed several times with deionized water after room temperature, and were dried in a vacuum drying oven at 60 °C for 4 h to obtain  $\text{Cr}_x\text{-Ni}(\text{OH})_2$ . Finally, the obtained  $\text{Cr}_x\text{-Ni}(\text{OH})_2$  and 0.4 g selenium powder were placed downstream and upstream of the quartz tube, respectively, and calcined at 300 °C for 2 h at a heating rate of 5 °C  $\text{min}^{-1}$  under nitrogen conditions. After cooling to room temperature,  $\text{Cr}_x\text{-NiSe}_2$  ( $x = 0.1, 0.25, 0.4$ ) is obtained. For comparison, Cr-NiO and  $\text{NiSe}_2$  were prepared using similar synthesis methods, but they were obtained without Se and Cr, respectively.

## 1. Structural characterizations

In X-ray diffraction (XRD) testing, samples are scraped from NF to rule out the influence of Ni substrate. The XRD data of the sample was obtained by using a Bruker D8 X-ray diffraction device with a tube voltage of 40 KV in the range of  $2\theta = 10\sim 80^\circ$ . Field emission scanning electron microscopy (SEM) measurements are performed by using a Thermo field Quattro S instrument to examine the surface morphology of the samples. High-resolution transmission electron microscopy (HRTEM) and transmission electron microscopy (TEM) were used to observe the microstructure details and elemental distribution of the material (JEM-F200). Thermo Fisher Scientific K-Alpha X-ray photoelectron spectroscopy (XPS) was used to investigate the valence state and chemical composition of the samples. Raman spectra were collected by using HORIBA XploRA Plus Raman imaging spectrometer, with a laser source wavelength of 532 nm, under natural conditions. Prior to testing, a 520  $\text{cm}^{-1}$  Raman peak of the silicon wafer was used for correction. In in-situ Raman measurements, Pt wire and Hg/HgO electrodes were used as the opposite electrode and the reference electrode, respectively. The controlled potential was applied to the catalyst in 1.0 M KOH+0.33 M urea solution, and Raman data was obtained at different potentials.

## 2. Electrochemical measurements

The electrochemical properties were measured by CHI 760E and CHI 660E electrochemical workstations. At room temperature, a standard three-electrode system was assembled with the self-supported electrodes (such

as Cr<sub>0.25</sub>-NiSe<sub>2</sub>, NiSe<sub>2</sub>, Cr-NiO) of loaded NF sample as the working electrode, graphite plate as the counter-electrode and Hg/HgO electrode as the reference electrode. Unless otherwise noted, the electrolyte was 1.0 M KOH+0.33 M urea solution with a pH of 14. For all samples, 80 cycles were performed to activate them by cyclic voltammetry (CV) at a rate of 100 mV s<sup>-1</sup> in the voltage range 0~1.0 V (vs. Hg/HgO). Subsequently, linear sweep voltammetry (LSV) was performed at a scan rate of 5 mV s<sup>-1</sup>, with 95%-iR correction compensated manually. Potential E (*RHE*) and overpotential  $\eta$  were calculated by the following formula:

$$E_{RHE} = E_{Hg/HgO} + 0.0592\text{pH} + 0.098 \text{ V} \quad (1)$$

$$\eta = E_{RHE} - 1.23 \quad (2)$$

The Tafel slope (b) was obtained from the LSV curve by using the Tafel equation:

$$\eta = b \log(j) + a \quad (3)$$

Where  $\eta$  is the overpotential and  $j$  is the corresponding current density. Cyclic voltammetry (CV) among -0.1 ~0.1 V vs. *RHE* was used to assess the electrochemical active area at the scan rates of 2, 4, 6, 8 and 10 mV s<sup>-1</sup> under the electric double layer capacitor ( $C_{dl}$ ). The equation is as follows:

$$C_{dl} = \frac{j_a - j_c}{2\nu} \quad (4)$$

Where  $\nu$  is the scanning rate,  $j_a$  is the positive scanning current density at 0 V (vs. Hg/HgO), and  $j_c$  is the negative scanning current density at 0 V (vs. Hg/HgO). Electrochemical impedance spectroscopy (EIS) was measured in the 0.01~100 kHz frequency range, the ac voltage was 5 mV, and the voltage was 1.4 V vs. *RHE*. The long-term durability of the catalyst was tested at constant current densities of 10 mA cm<sup>-2</sup> and 100 mA cm<sup>-2</sup> for 100 hours.

### 3. DFT methods

In the present study, all computational tasks were executed utilizing the DMol3 module within Materials Studio3.<sup>1</sup> [Delley, B. An all-electron numerical method for solving the local density functional for polyatomic molecules. *J. Chem. Phys.* 92, 508-517 (1990).] Upon achieving an energy convergence tolerance of  $1 \times 10^{-5}$  Hartree, a maximum force convergence threshold of 0.004 Hartree per Angstrom (1 Angstrom being equivalent to  $1 \times 10^{-10}$  meters), and a maximum displacement convergence of 0.005 Angstrom. The pertinent energy calculations and geometric structure optimizations were deemed complete. The electron exchange and correlation functions were modeled using the Perdew-Burke-Ernzerhof (PBE) generalized gradient

approximation (GGA) functional.<sup>2</sup> [Perdew, J. P. Generalized gradient approximations for exchange and correlation: A look backward and forward. *Phys. B* 172, 1-6 (1991).] A vacuum slab with a thickness of 15 Angstroms was employed to segregate the surface, thereby preventing inter-layer interactions, with the symmetry parameters set to none and spin polarization configured as Collinear. The Brillouin zone's k-point was established at  $2 \times 2 \times 1$ , and a global orbital cutoff radius of 4.4 Angstroms was implemented.

The adsorption energy ( $E_{\text{ads}}$ ) of urea intermediates for all models is calculated according to the following formula:

$$\Delta E_{\text{ads}} = E_{\text{oxy/mod}} - E_{\text{oxy}} - E_{\text{mod}} \quad (5)$$

Where  $\Delta E_{\text{ads}}$  represents the adsorption energy of urea intermediates on active site,  $E_{\text{oxy/mod}}$  represents the total energy of the model with urea intermediates, and  $E_{\text{oxy}}$  represents the energy of oxygen intermediates.  $E_{\text{mod}}$  is the energy of models. The free energy ( $\Delta G$ ) of the reaction steps is calculated by using the calculated hydrogen electrode model. The  $\Delta G$  of the reaction step is calculated as follows:

$$\Delta G = \Delta E_{\text{ads}} + \Delta E_{\text{ZPE}} + T\Delta S \quad (6)$$

Where  $\Delta E_{\text{ZPE}}$  is the differences in the zero-point energy,  $\Delta S$  is the change of entropy, and T is the temperature (T = 298 K), respectively.

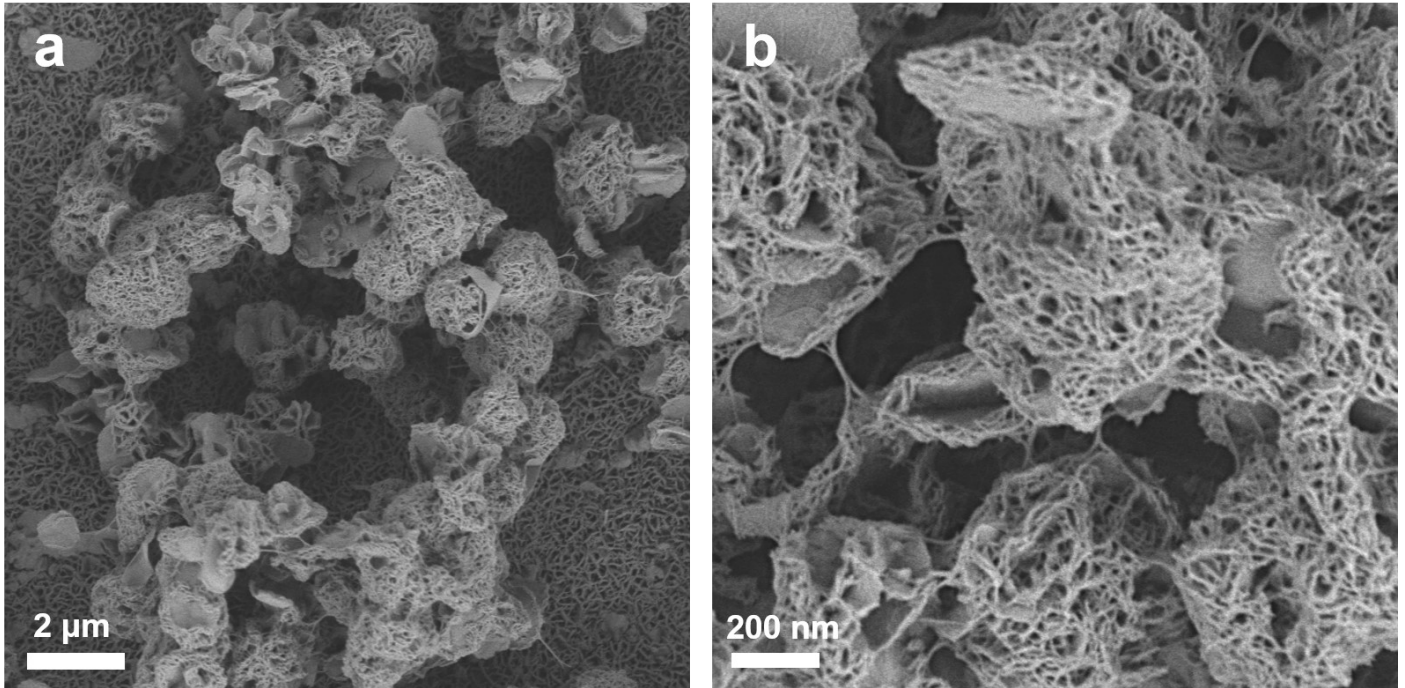


**Fig. S1.** (a-b) SEM images of NiSe<sub>2</sub> with different magnifications.

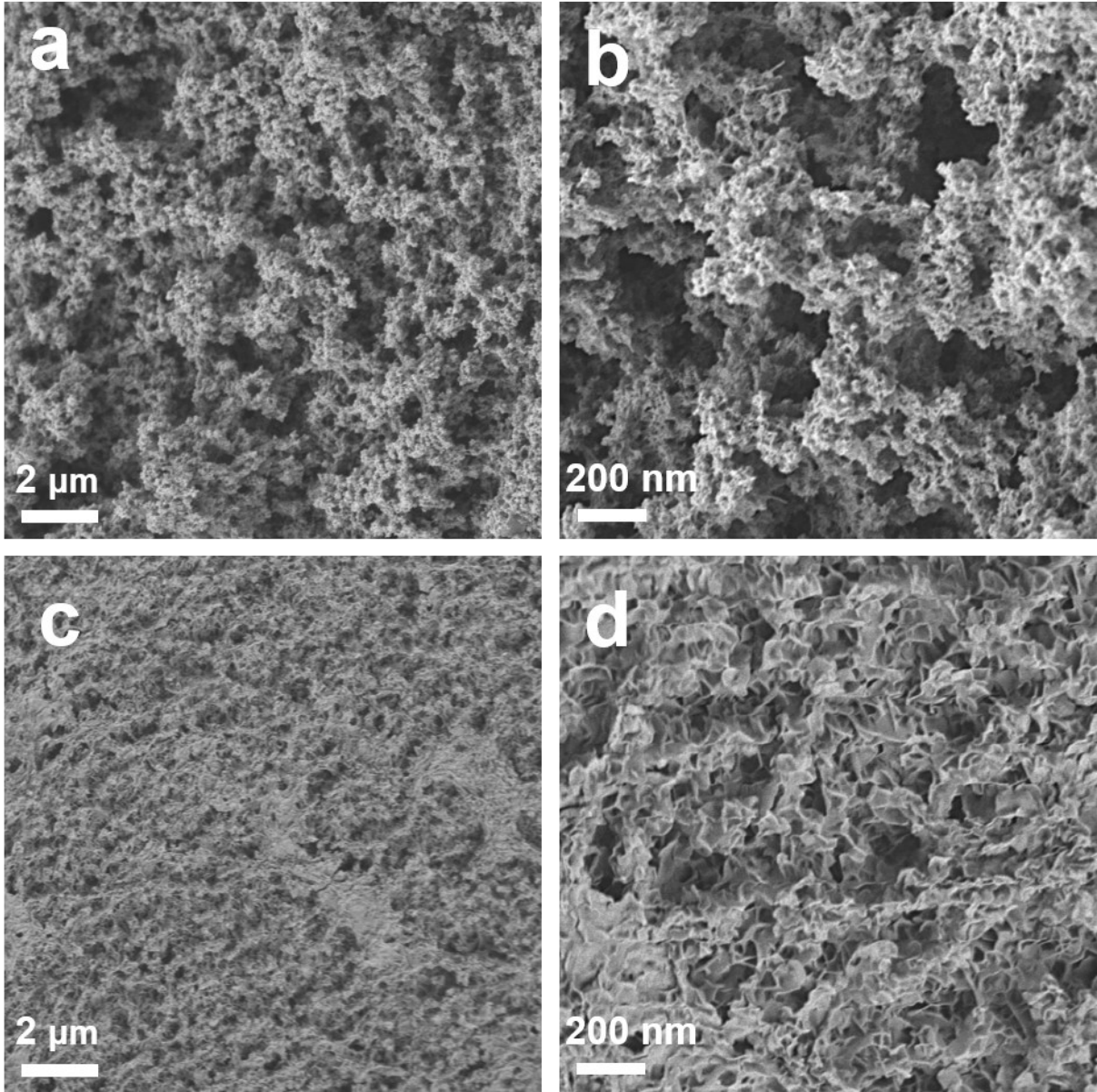


**Fig. S2.** (a-b) SEM images of  $\text{Cr}_{0.1}\text{-NiSe}_2$  with different magnifications; (c-d) SEM images of  $\text{Cr}_{0.4}\text{-NiSe}_2$  with different magnifications.

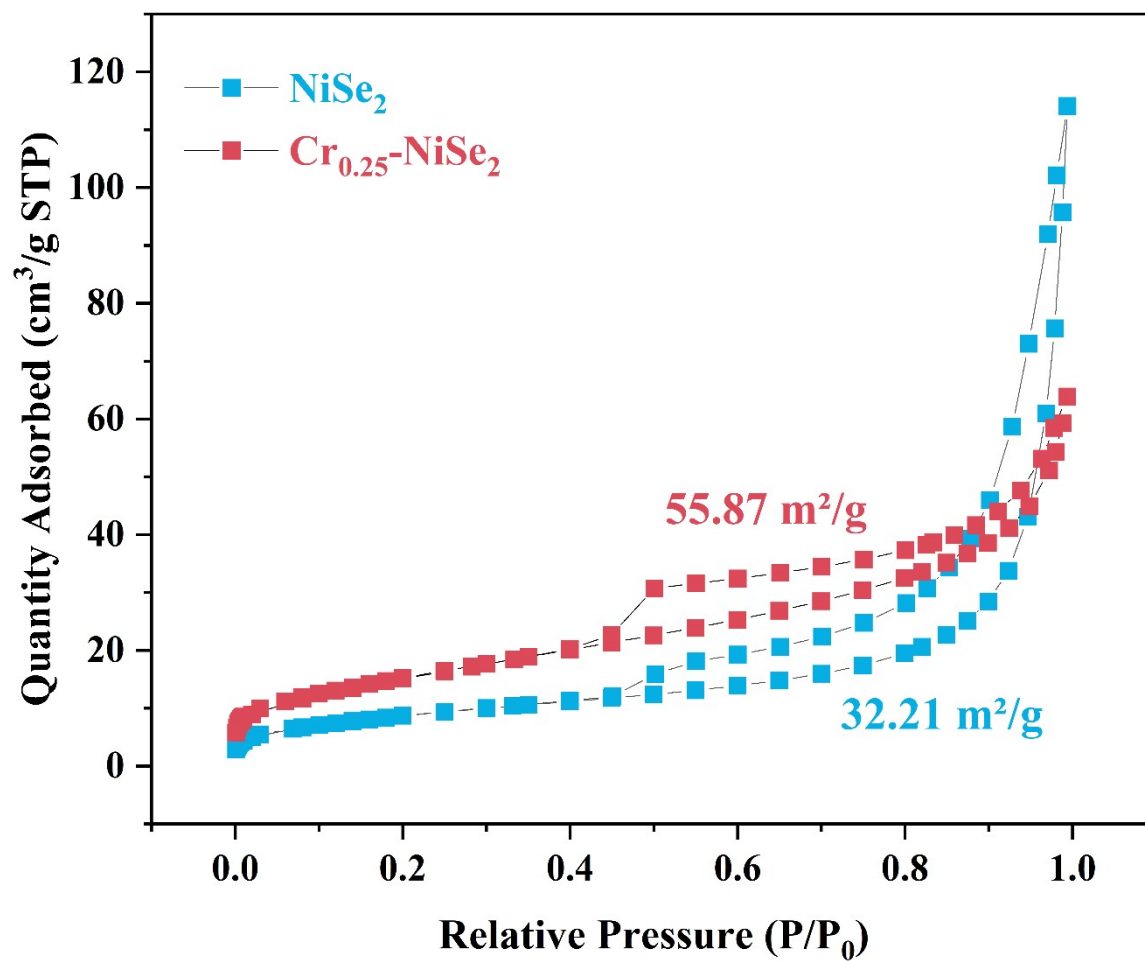


Fig. S3. N<sub>2</sub> adsorption/desorption isotherms of NiSe<sub>2</sub> and Cr<sub>0.25</sub>-NiSe<sub>2</sub>.

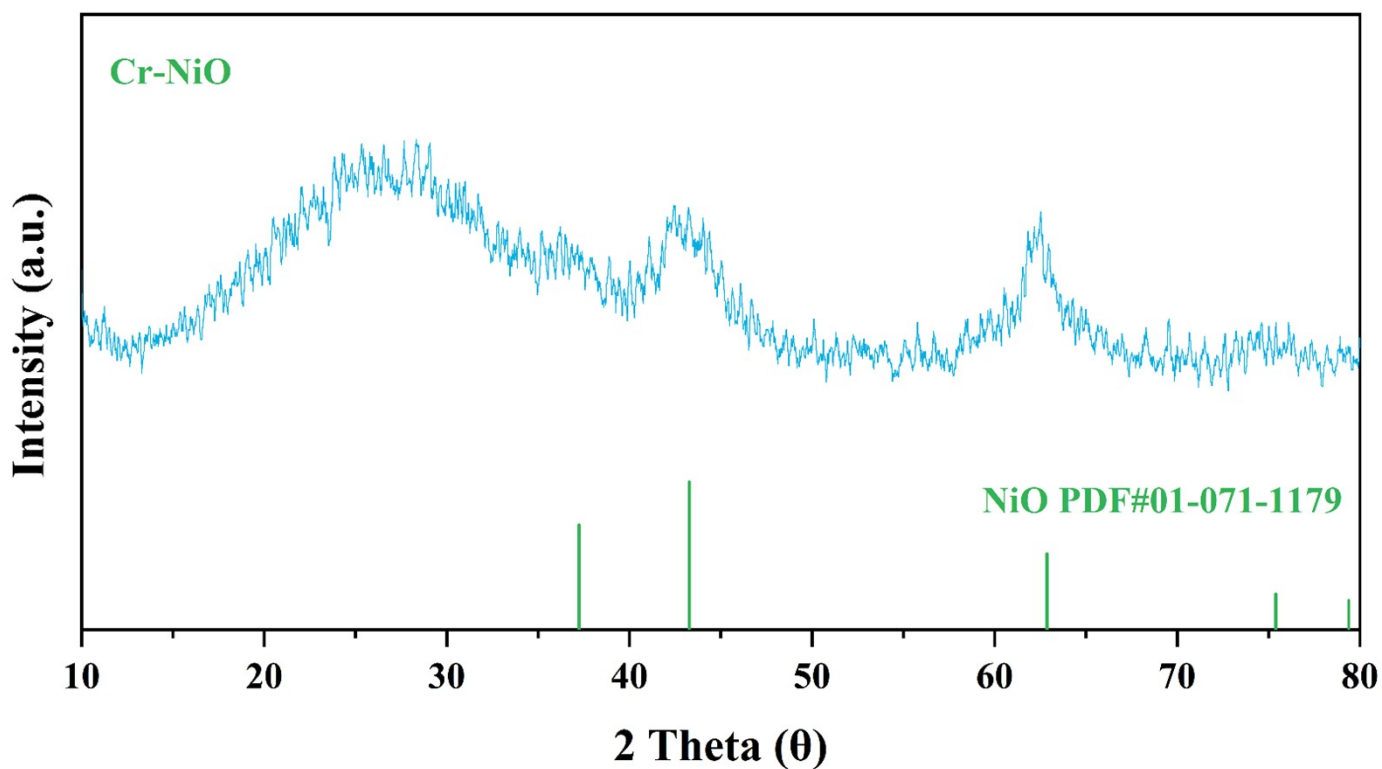


Fig. S4. XRD pattern of Cr-NiO sample.

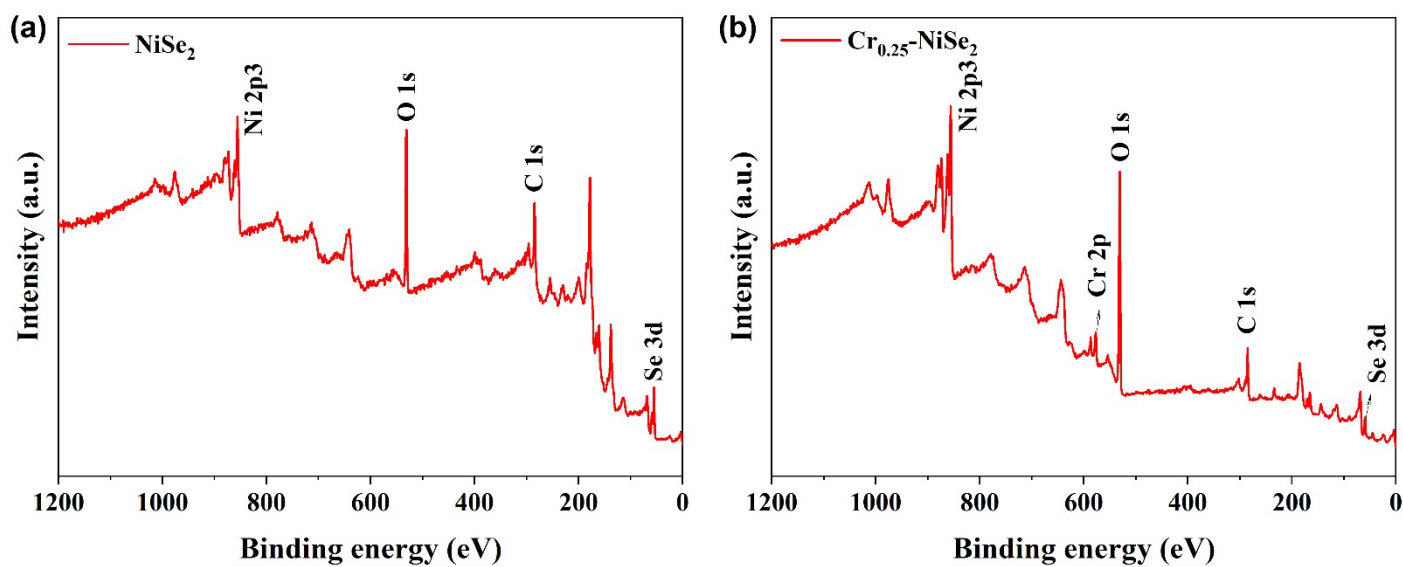


Fig. S5. XPS survey spectra of (a) NiSe<sub>2</sub>, and (b) Cr<sub>0.25</sub>-NiSe<sub>2</sub>.

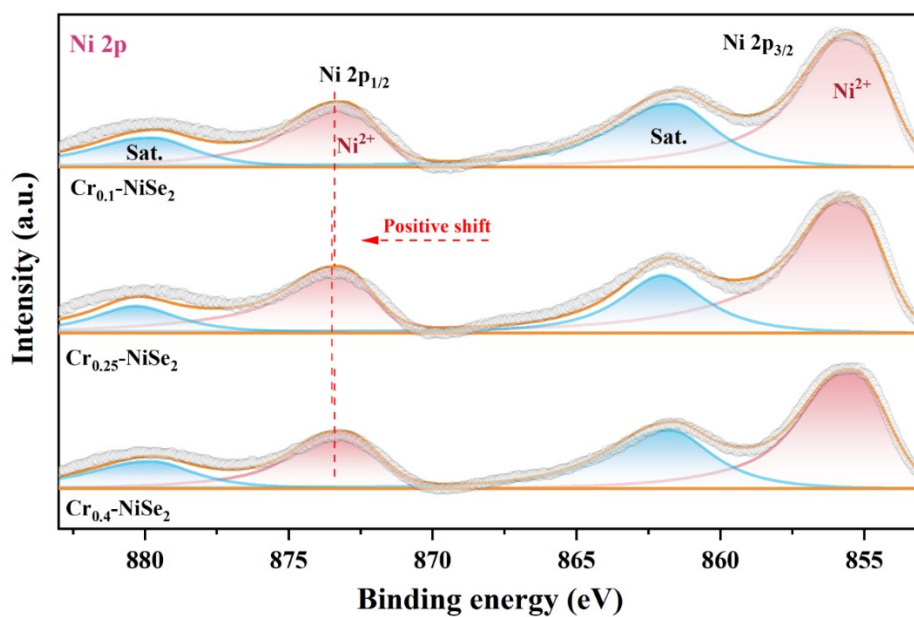


Fig. S6. High-resolution XPS spectra of Ni 2p of  $\text{Cr}_{0.1}\text{-NiSe}_2$ ,  $\text{Cr}_{0.25}\text{-NiSe}_2$ , and  $\text{Cr}_{0.4}\text{-NiSe}_2$ .

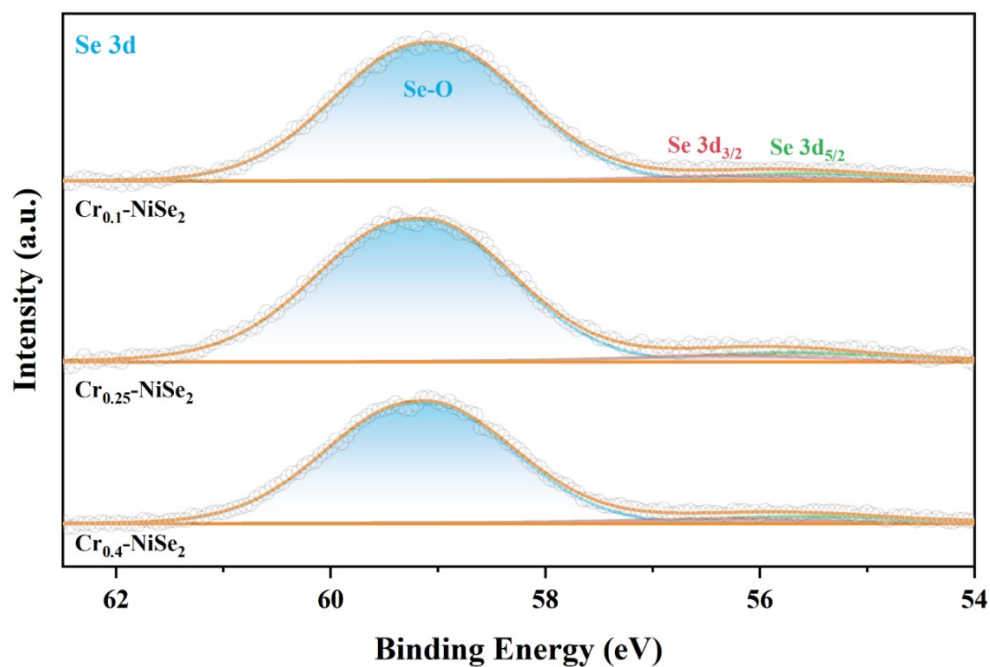
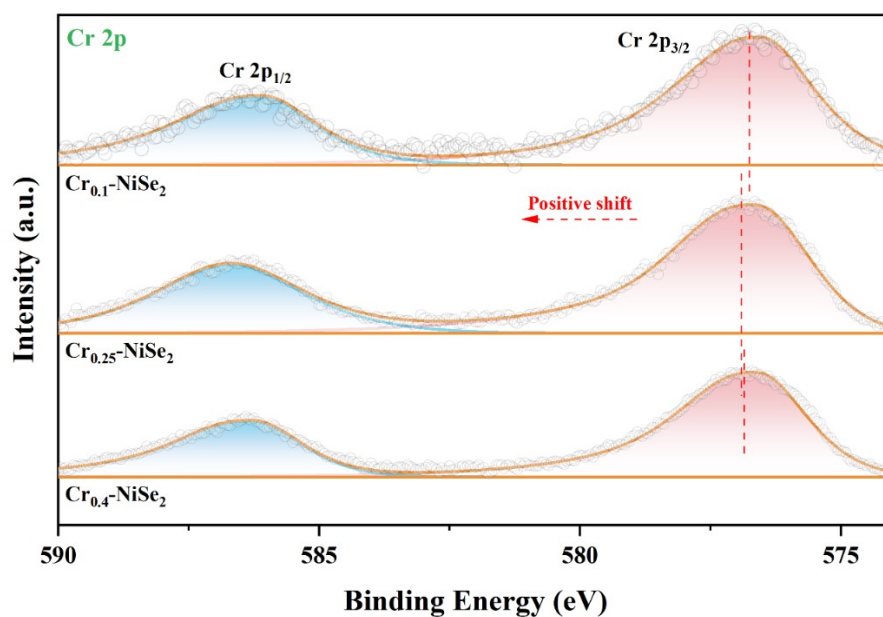
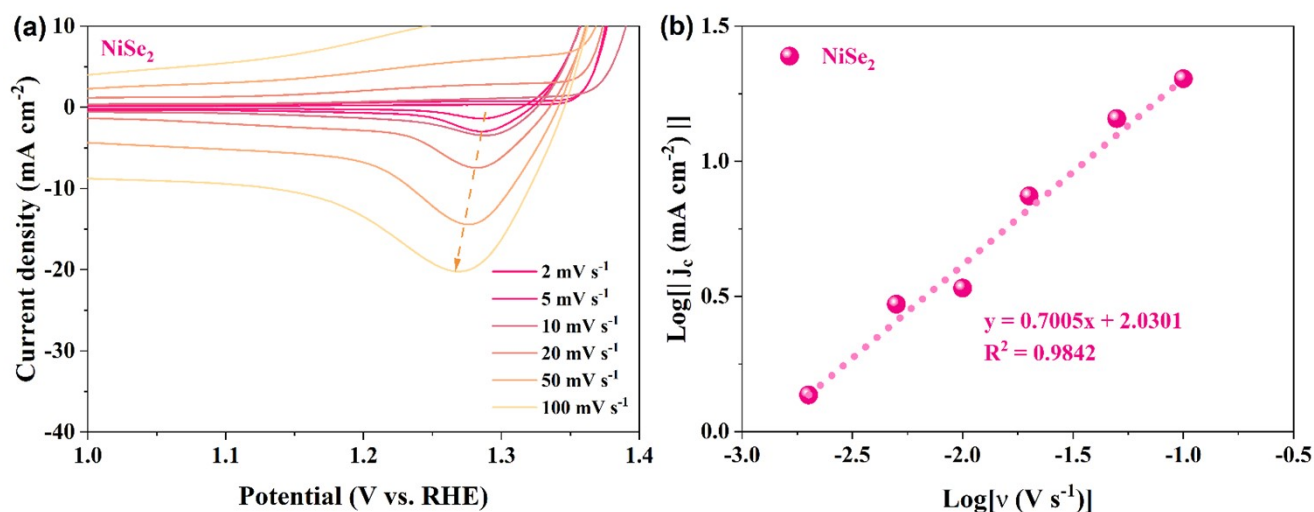


Fig. S7. High-resolution XPS spectra of Se 3d of  $\text{Cr}_{0.1}\text{-NiSe}_2$ ,  $\text{Cr}_{0.25}\text{-NiSe}_2$ , and  $\text{Cr}_{0.4}\text{-NiSe}_2$ .



**Fig. S8.** High-resolution XPS spectra of Cr 2p of  $\text{Cr}_{0.1}\text{-NiSe}_2$ ,  $\text{Cr}_{0.25}\text{-NiSe}_2$ , and  $\text{Cr}_{0.4}\text{-NiSe}_2$ .



**Fig. S9.** (a) Cyclic voltammograms of  $\text{NiSe}_2$  in 1 M KOH+0.33 M urea solution at different scan rates; (b) Plot of the logarithm of cathodic peak current density ( $j_c$ ) against the logarithm of scan rate ( $v$ ).

The given cathode current density  $j_c$  and the sweep rate  $v$  obey a power-law relationship:  $j_c = av^b$ ,<sup>3, 4</sup> where  $a$  and  $b$  are both adjustable parameters, and the  $b$  value is determined by the slope of the  $\text{Log}j_c$  vs  $\text{Log}v$  curve. There are two limit cases,  $b = 0.5$  and  $b = 1$ . (i) when  $b = 0.5$ , it indicates that the redox process is controlled by diffusion; (ii) When it is a fully non-diffusion-controlled capacitive behavior,  $b = 1$ . Combined with Fig.

S9, the b value is 0.7005, indicating that the redox characteristics are related to the mixed control of diffusion and capacitance behavior, similar to  $\text{Cr}_{0.25}\text{-NiSe}_2$ .

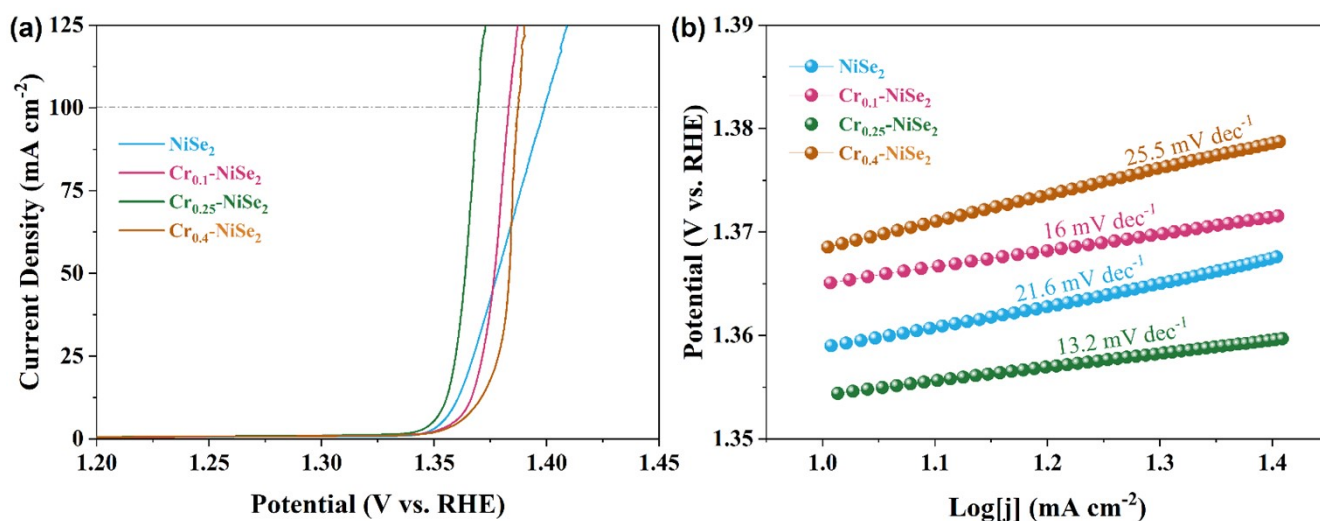


**Fig. S10.** (a) LSV curves and (b) Tafel plots of  $\text{Cr}_{0.1}\text{-NiSe}_2$ ,  $\text{Cr}_{0.25}\text{-NiSe}_2$ , and  $\text{Cr}_{0.4}\text{-NiSe}_2$  samples in 1.0 M KOH+0.33 M urea.

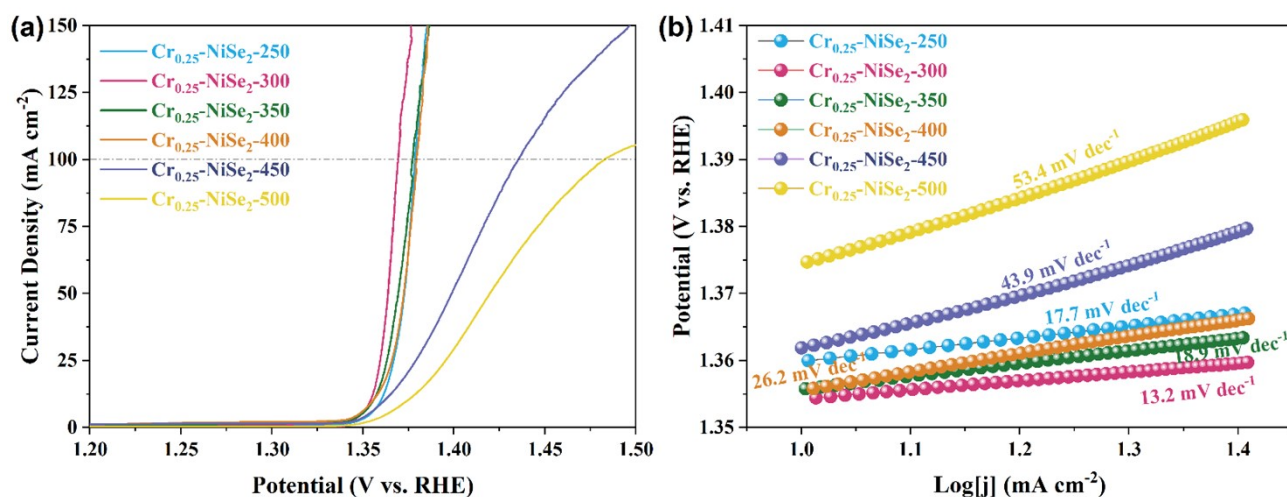


**Fig. S11.** (a) LSV curves and (b) Tafel plots of  $\text{Cr}_{0.25}\text{-NiSe}_2$  sample in 1.0 M KOH+0.33 M urea ( $\text{Cr}_{0.25}\text{-NiSe}_2$  sample were obtained at different selenization temperature of 250 $^{\circ}\text{C}$ , 300  $^{\circ}\text{C}$ , 350  $^{\circ}\text{C}$ , 400  $^{\circ}\text{C}$  and 500  $^{\circ}\text{C}$ ).

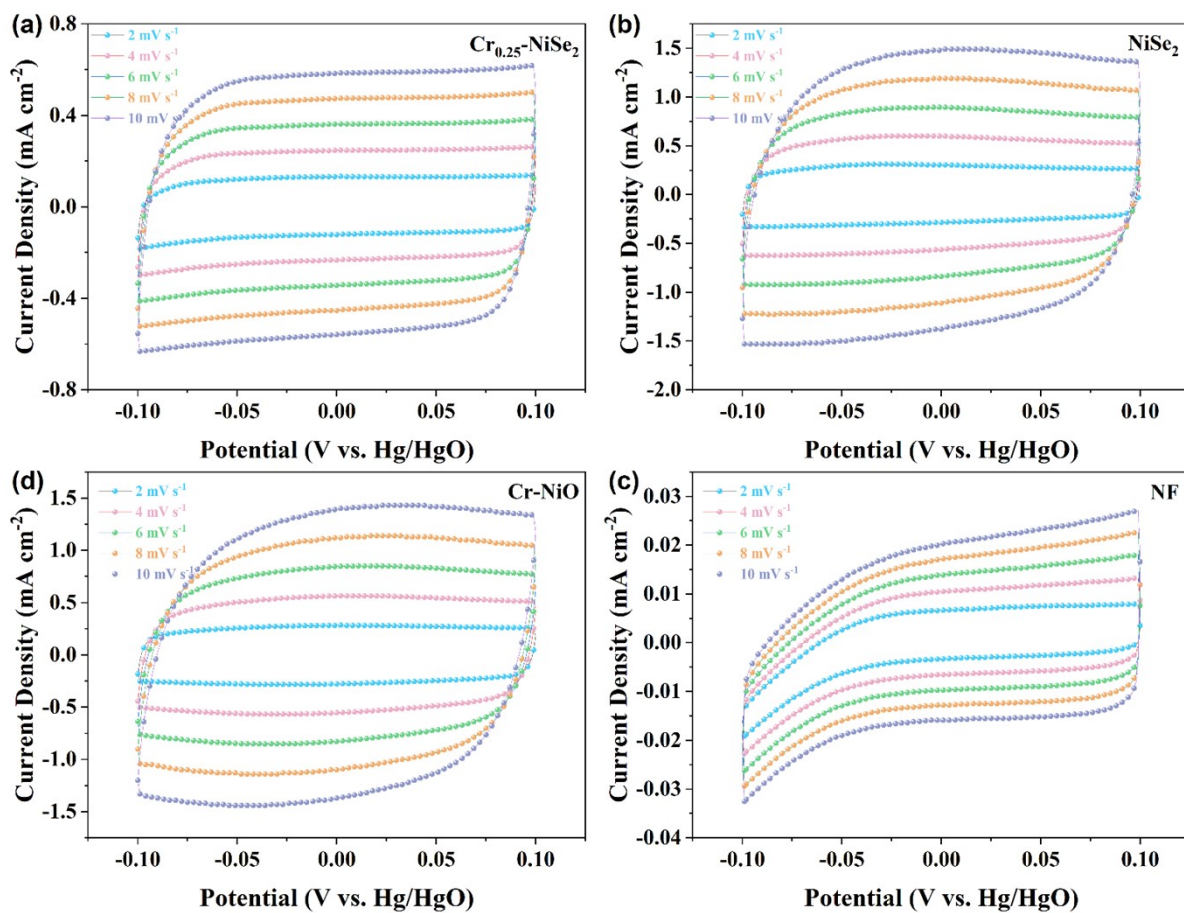


**Fig. S12.** CVs of (a)  $\text{Cr}_{0.25}\text{-NiSe}_2$ , (b)  $\text{NiSe}_2$ , (c)  $\text{Cr-NiO}$ , and (d) NF at different scan rates from 2 to  $10 \text{ mVs}^{-1}$ .

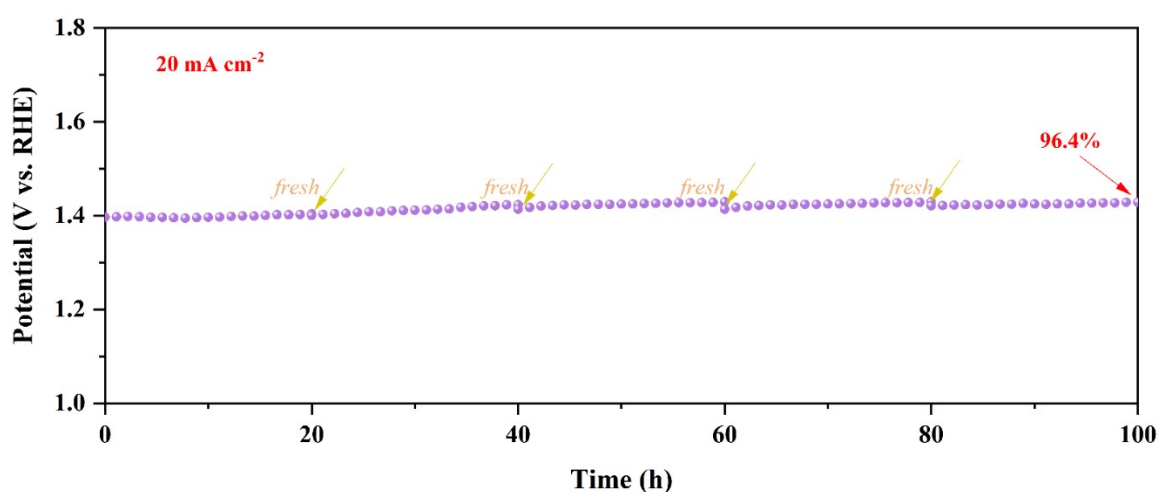


**Fig. S13.** Stability test of  $\text{Cr}_{0.25}\text{-NiSe}_2$  at  $j = 20 \text{ mA cm}^{-2}$  in  $1.0 \text{ M KOH} + 0.33 \text{ M urea}$  ("fresh" indicates the replacement of the electrolyte).

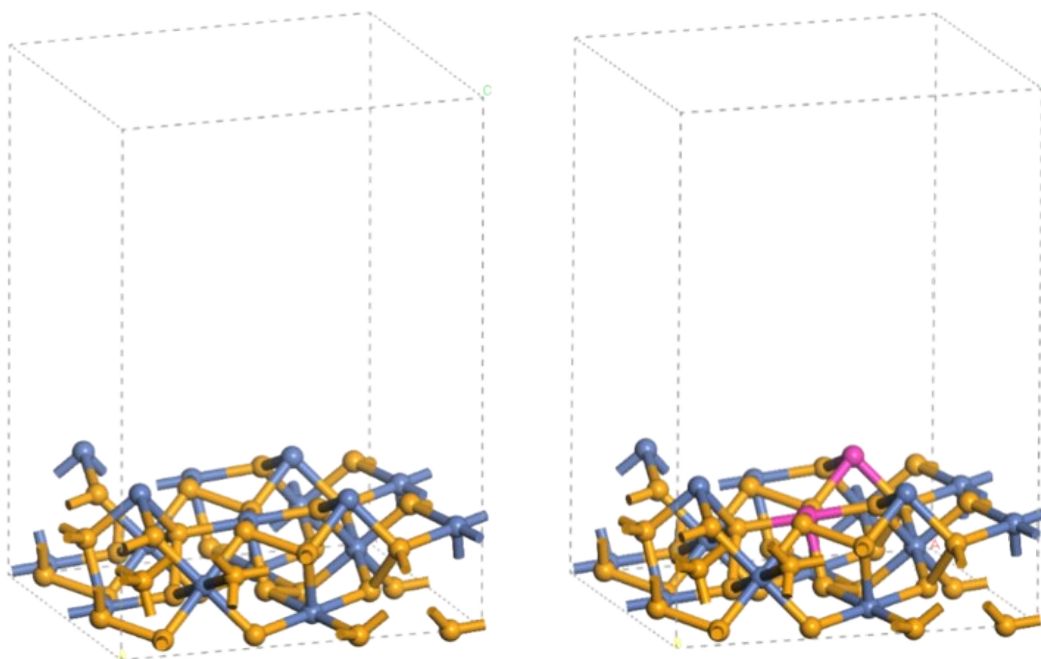


**Fig. S14.** Schematic diagram of crystal structure of NiSe<sub>2</sub> and Cr<sub>0.25</sub>-NiSe<sub>2</sub>.

**Table S1.** Impedance fitting results of as-prepared Cr<sub>0.25</sub>-NiSe<sub>2</sub> comparing with different catalytic electrodes, the impedance test was carried out in a solution of 1 M KOH with 0.33 M urea.

	<b>Cr<sub>0.25</sub>-NiSe<sub>2</sub></b>	<b>NiSe<sub>2</sub></b>	<b>Cr-NiO</b>	<b>NF</b>
<b>Rs (Ω)</b>	<b>1.342</b>	1.184	1.256	1.031
<b>Rct (Ω)</b>	<b>4.213</b>	5.024	4.904	17.65

**Table S2.** Comparison of UOR performances of Cr<sub>0.25</sub>-NiSe<sub>2</sub> with other recently reported transition metal chalcogenides catalysts.

catalyst	Potential (V vs. RHE) for 100 mA cm <sup>-2</sup>	Tafel slope (mV dec <sup>-1</sup> )	Electrolyte	Ref
<b>Cr<sub>0.25</sub>-NiSe<sub>2</sub></b>	<b>1.37</b>	<b>13.2</b>	<b>1 M KOH + 0.33 M Urea</b>	<b>This work</b>
CoFeCr LDH/NF	1.4	85	1M KOH + 0.33 M Urea	5
NiSe <sub>2</sub> /MoSe <sub>2</sub>	1.38	20.13	1 M KOH + 0.5 M Urea	6
MoSe <sub>2</sub> /NiSe <sub>2</sub>	1.47	68	1.M KOH + 0.5 M Urea	7
Ni-TPA@NiSe/NF	1.37	22.7	1.M KOH + 0.5 M Urea	8
NiCoCr-LDH/NF	1.38	18.61	1.M KOH + 0.5 M Urea	9
NiSe@Ni <sub>12</sub> P <sub>5</sub> /NCF	1.412	53.65	1.M KOH + 0.5 M Urea	10
Cr-Ni(OH) <sub>2</sub>	1.38	14	1.M KOH + 0.33 M Urea	11
Fe-Ni <sub>2</sub> PNiSe <sub>2</sub> -12	1.39	28	1.M KOH + 0.33 M Urea	12
Cr、P-NiMoO <sub>4</sub> @NF	1.39	8.12	1.M KOH + 0.5 M Urea	13
PBA@MOF-Ni/Se	1.42	64	1.M KOH + 0.5 M Urea	14
Ni <sub>0.86</sub> Se-NiSe <sub>2</sub> @NC-2	1.41	64.4	1M KOH + 0.33 M Urea	15
Ni <sub>3</sub> S <sub>3</sub> -Cr(OH) <sub>3</sub> - Ti <sub>3</sub> C <sub>2</sub> @NF	1.38	14.99	1.M KOH + 0.5 M Urea	16

**Table S3.** Comparison of the overall urea splitting performance of Cr<sub>0.25</sub>-NiSe<sub>2</sub> || Pt/C with the reported catalysts.

catalyst	Potential (V) for 10 mA cm <sup>-2</sup>	Stability (h)	Ref
<b>Cr<sub>0.25</sub>-NiSe<sub>2</sub>    Pt/C</b>	<b>1.42</b>	<b>20</b>	<b>This work</b>
a-FeCoO	1.54	36	17
Ce-NiVS	1.55	15	18
Cu-doped Ni <sub>3</sub> S <sub>2</sub> /NF	1.57	-	19
NiS/MoS <sub>2</sub> @CC	1.46	25	20
N-NiS/NiS <sub>2</sub>	1.61	8	21
NP-Ni <sub>0.7</sub> Fe <sub>0.3</sub>	1.55	10	22
V-Co <sub>2</sub> P <sub>4</sub> O <sub>12</sub> /CC	1.42	20	23

## References

1. B. Delley, *J. Chem. Phys.*, 1990, **92**, 508-517.
2. J. P. Perdew, *Physica B*, 1991, **172**, 1-6.
3. T. Brezesinski, J. Wang, J. Polleux, B. Dunn and S. H. Tolbert, *J. Am. Chem. Soc.*, 2009, **131**, 1802-1809.
4. Z. Xu, Q. Chen, Q. Chen, P. Wang, J. Wang, C. Guo, X. Qiu, X. Han and J. Hao, *J. Mater. Chem. A*, 2022, **10**, 24137-24146.
5. Z. Wang, W. Liu, Y. Hu, M. Guan, L. Xu, H. Li, J. Bao and H. Li, *Appl. Catal. B-Environ. Energy*, 2020, **272**, 118959.
6. X. Xu, H. Liao, L. Huang, S. Chen, R. Wang, S. Wu, Y. Wu, Z. Sun and H. Huang, *Appl. Catal. B-Environ. Energy*, 2024, **341**, 123312.
7. Y. Chen, J. Ge, Y. Wang, X. Zhao, F. Zhang and X. Lei, *ACS Appl. Nano Mater.*, 2024, **7**, 12091-12100.
8. L. Jin, R. Ji, H. Wan, J. He, P. Gu, H. Lin, Q. Xu and J. Lu, *ACS Catal.*, 2023, **13**, 837-847.

9. S. Xu, D. Jiao, X. Ruan, Z. Jin, Y. Qiu, Z. Feng, L. Zheng, J. Fan, W. Zheng and X. Cui, *Adv. Funct. Mater.*, 2024, **34**, 2401265.
10. M. Li, J. Wang, J. Liao, L. Wang, Y. Ju, X. Wang, J. Wei, N. Hu, R. Xu and L. Yang, *Appl. Surf. Sci.*, 2023, **607**, 155041.
11. J. Zhang, X. Song, L. Kang, J. Zhu, L. Liu, Q. Zhang, D. J. L. Brett, P. R. Shearing, L. Mai, I. P. Parkin and G. He, *Chem. Catalysis*, 2022, **2**, 3254-3270.
12. C.-J. Huang, Q.-N. Zhan, H.-M. Xu, H.-R. Zhu, T.-Y. Shuai and G.-R. Li, *Inorg. Chem.*, 2024, **63**, 8925-8937.
13. M. Liu, H. Zhao, X. Du and X. Zhang, *Int. J. Hydrog. Energy*, 2023, **48**, 38143-38155.
14. H. Xu, K. Ye, K. Zhu, Y. Gao, J. Yin, J. Yan, G. Wang and D. Cao, *Inorg. Chem. Front.*, 2021, **8**, 2788-2797.
15. Q. Cao, W. Huang, J. Shou, X. Sun, K. Wang, Y. Zhao, R. Ding, W. Lin, E. Liu and P. Gao, *J. Colloid Interface Sci.*, 2023, **629**, 33-43.
16. Y. Liu, Q. Chen and Q. Zhong, *Nanoscale*, 2023, **15**, 14131-14139.
17. T. Wei, G. Meng, Y. Zhou, Z. Wang, Q. Liu, J. Luo and X. Liu, *Chem. Commun.*, 2023, **59**, 9992-9995.
18. C. Wang, Q. Wang, X. Du and X. Zhang, *Dalton Trans.*, 2023, **52**, 13161-13168.
19. M. Wei, D. Zhang, J. Deng, X. Xiao, L. Wang, X. Wang, M. Song, S. Wang, X. Zheng and X. Liu, *Ind. Eng. Chem. Res.*, 2022, **61**, 7777-7786.
20. C. Gu, G. Zhou, J. Yang, H. Pang, M. Zhang, Q. Zhao, X. Gu, S. Tian, J. Zhang, L. Xu and Y. Tang, *Chem. Eng. J.*, 2022, **443**, 136321.
21. H. Liu, Z. Liu, F. Wang and L. Feng, *Chem. Eng. J.*, 2020, **397**, 125507.
22. Z. Cao, T. Zhou, X. Ma, Y. Shen, Q. Deng, W. Zhang and Y. Zhao, *ACS Sustain. Chem. Eng.*, 2020, **8**, 11007-11015.
23. X.-W. Chang, S. Li, L. Wang, L. Dai, Y.-P. Wu, X.-Q. Wu, Y. Tian, S. Zhang and D.-S. Li, *Adv. Funct. Mater.*, 2024, **34**, 2313974.